ChemComm

ROYAL SOCIETY OF CHEMISTRY

COMMUNICATION

View Article Online
View Journal | View Issue

Cite this: *Chem. Commun.*, 2024, **60**, 11964

Received 1st August 2024,
Accepted 24th September 2024

DOI: 10.1039/d4cc03901g

rsc.li/chemcomm

Fullerene as a probe molecule for single-atom oxygen reduction electrocatalysts†

Ning Li,‡[a] Kun Guo, ‡*[a] Song Lu,[b] Lipiao Bao, [a] Zhixin Yu [c] and Xing Lu *[a]

Fullerenes interact positively with many metal-based catalysts *via* intense electron transfer. Yet, we here revealed that C_{60} serves as a probe due to its deactivation of the active sites of single-atom O_2 reduction electrocatalysts. C_{60} adsorption to metal atoms creates steric hindrance that restricts the access of O_2 to the active sites.

Fullerenes are π-conjugated molecular carbon allotropes with a set of fascinating structural and electronic properties that have triggered significant interest from the catalysis community.[1–3] For instance, the abundant native pentagons render fullerenes an unparalleled feedstock to construct intrinsic defect-rich carbon catalysts.[4–6] The metal-like electrical conductivity brings higher fullerene C_{96} with superior oxygen reduction reaction (ORR) activity to that of semiconducting C_{60} and C_{70}.[7] Besides, covalent 2D fullerene networks with suitable band gaps and high carrier mobility are potent photocatalysts for water splitting.[8,9]

Recently, fullerenes as powerful regulators of the localized electronic structures of metal-based catalysts are increasingly being reported. For example, the exceptional redox capability renders C_{60} molecules as a robust electron-buffering agent between Cu^0/Cu^+ and Cu^{2+}/Cu^+ couples.[10] Compared to Cu/SiO_2 with dominant Cu^0 species, C_{60} can extract electrons from Cu^0 to form C_{60}^- and Cu^+. Meanwhile, C_{60}^- can also donate electrons to Cu^{2+}, forming C_{60} and Cu^+. As a result, crucial Cu^+ species are stabilized by C_{60} to enhance the hydrogenation activity of C_{60}-Cu/SiO_2. In pursuit of the monovalent Cu^+ species that play a pivotal role in Cu-based catalysts towards CO_2 electroreduction, researchers have devised C_{60}-adsorbed Cu metals as superior electrocatalysts to bare Cu.[11,12] Likewise, intense interfacial electron transfer induced by fullerene molecules has also been evidenced to enhance the catalytic performance of metallic substrates, such as CoNi layered double hydroxides[13] and MoS_2.[14,15] Nevertheless, positive electronic interactions are uncovered only between fullerenes and large-sized metallic aggregates. How sub-nanoscale fullerenes would affect the metal active sites at the atomic level remains an unresolved issue. It is thus of high interest to explore whether fullerenes can still optimize the electronic structure of the metal site where they are adsorbed to, behaving like a feasible axial ligand of metal single-atom catalysts (SACs).[16–21] Or alternatively, the larger sizes of fullerene molecules than that of metal atoms may result in the deactivation of the metal site by surface blocking, functioning as a molecular probe of the active site of SACs.

Macrocycles bearing representative $M–N_4–C$ moieties have been widely exploited as model catalysts to investigate various carbon-hosted SACs.[22–24] Utilizing metalloporphyrin (MP) as a molecular SAC, we unravel the unexpected inhibiting effect of C_{60} in the ORR activity of MP. Control experiments indicate that non-covalently anchoring either cobalt porphyrin (CoP) or C_{60} on carbon nanotubes (CoP/CNT and C_{60}/CNT) leads to much higher ORR activity than individual CoP, C_{60}, and CNTs. However, further addition of C_{60} to CoP/CNT (C_{60}-CoP/CNT) results in a dramatic ORR activity decay, the same as that observed after adding the well-noted thiocyanate (SCN^-) poison. Density functional theory (DFT) calculations reveal that the planar MP molecule is confined between the CNT matrix and C_{60} molecule, creating high steric hindrance that restricts O_2 access to the active Co atoms.

CoP/CNT and C_{60}-CoP/CNT are prepared *via* a straightforward π interaction-enabled adsorption strategy by mixing different precursors in CS_2 solvent (Experimental section, ESI†). In particular, CoP is selected because it presents better ORR activity than the other common 3d metal MPs (Fig. S1, ESI†).[25]

---

[a] *State Key Laboratory of Materials Processing and Die & Mould Technology, School of Materials Science and Engineering, Huazhong University of Science and Technology, Wuhan 430074, China. E-mail: guok@hust.edu.cn, lux@hust.edu.cn*

[b] *Institute of New Energy, School of Chemistry and Chemical Engineering, Shaoxing University, Shaoxing 312000, China*

[c] *Department of Energy and Petroleum Engineering, University of Stavanger, Stavanger 4036, Norway*

† Electronic supplementary information (ESI) available: Experimental section, characterization and electrochemical data. See DOI: **https://doi.org/10.1039/d4cc03901g**

‡ These authors contributed equally to this work.

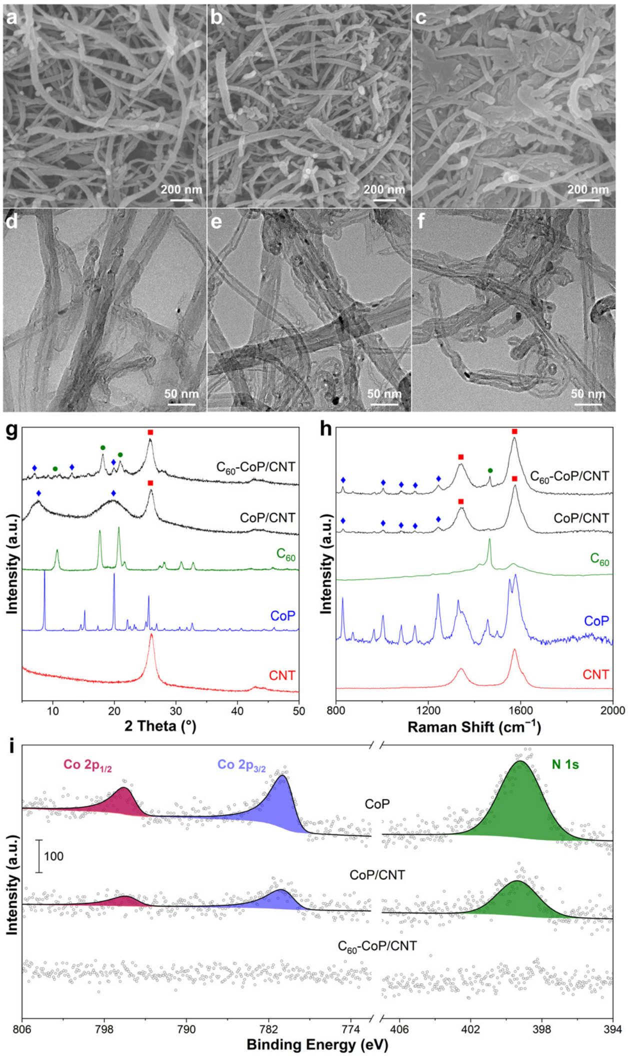

Fig. 1 SEM (a)–(c) and TEM (d)–(f) images of the CNTs (a) and (d), CoP/CNT (b) and (e), and C_{60}-CoP/CNT (c) and (f). XRD patterns (g) and Raman spectra (h) of the CNTs, CoP, C_{60}, CoP/CNT, and C_{60}-CoP/CNT. The red square, blue rhombus, and green circle in (g) and (h) represent CNT, CoP, and C_{60}, respectively. (i) XPS spectra of the Co 2p and N 1s regions of CoP, CoP/CNT, and C_{60}-CoP/CNT.

The mass loading of CoP is optimized to be 50 wt% due to the highest ORR activity among a series of CoP/CNT (Fig. S2, ESI†). The same molar quantity of C_{60} as that of CoP is then added in C_{60}-CoP/CNT. The morphology and structure of the as-prepared materials are first examined by scanning and transmission electron microscopies (SEM and TEM). The typical 1D morphology is clearly seen in the commercially-received CNTs (Fig. 1a). Despite the high tendency for the self-assembly of CoP and C_{60} into large molecular crystals, no obvious aggregates are discerned in either CoP/CNT (Fig. 1b) or C_{60}-CoP/CNT (Fig. 1c), which could be attributed to the improved dispersity of both molecules on CNTs. This is further supported by their TEM images. It is found that these CNTs are composed of multi-walled tubes with diameters of dozens of nanometers (Fig. 1d). The uniform image contrasts indicate the absence of large-sized crystalline particles in CoP/CNT (Fig. 1e) and C_{60}-CoP/CNT (Fig. 1f). Additional SEM and TEM images are presented in Fig. S3 (ESI†).

The crystallinity of the materials under study is investigated by X-ray diffraction (XRD). As shown in Fig. 1g, a major characteristic peak at ∼26°, corresponding to the (002) plane of graphitic carbon, is observed for the CNTs. Pure CoP and C_{60} show well-defined characteristic peaks, reflecting the fact that they are easily self-assembled into crystalline particles owing to intermolecular forces.[26] After loading CoP on the CNTs, aside from the diffraction peak of the CNTs, two broad peaks that can be assigned to CoP are discerned, indicating the significantly decreased crystallinity of CoP. A similar phenomenon is also observed after further addition of C_{60} to form C_{60}-CoP/CNT, in which the C_{60} phase presents much lower crystallinity than pure C_{60}. The results again manifest that CNTs substantially mitigates the severe aggregation of CoP and C_{60} molecules.[27]

Raman spectroscopy is further employed to analyze the chemical structures of these materials. Typical D and G bands of graphitic carbon materials at 1340 and 1570 cm^{-1} are observed for CNTs, CoP/CNT, and C_{60}-CoP/CNT (Fig. 1h). Besides, multiple weak Raman bands originating from CoP are also observed in CoP/CNT, whereas an additional band at 1460 cm^{-1}, namely the $A_g(2)$ mode of C_{60}, is discerned in C_{60}-CoP/CNT. The Raman results also confirm that only small-sized CoP and C_{60} aggregates are formed after their hybridization with CNTs. Elemental states and speciation information of CoP, CoP/CNT, and C_{60}-CoP/CNT are further acquired by X-ray photoelectron spectroscopy (XPS). The full-survey XPS spectra verify the existence of C, N, and Co elements (Fig. S4, ESI†). Fig. 1i displays the high-resolution XPS spectra of the Co 2p and N 1s regions, in which the Co 2p spectra can be resolved into two spin–orbit doublets, Co $2p_{1/2}$ and Co $2p_{3/2}$, whereas the peak centered at 399.2 eV can be assigned to the pyrrolic N of CoP. Compared to CoP, the intensities of the Co $2p_{1/2}$, Co $2p_{3/2}$, and N 1s peaks for CoP/CNT become substantially lower, coinciding with the lower mass ratio of CoP in CoP/CNT. Importantly, the Co 2p and N 1s peaks are barely observable for C_{60}-CoP/CNT, indicating that the addition of C_{60} may lead to the surface coverage of CoP to a certain depth that is beyond the detection limit of XPS.

The ORR performance of the catalysts under study is then evaluated using the standard rotating disk electrode technique in 0.1 M KOH electrolyte (pH = 13). Fig. 2a shows the polarization curves of the ORR on six different catalysts at 1600 rpm. Their corresponding half-wave potentials ($E_{1/2}$) are measured and compared in Fig. 2b. Either C_{60} or CNT alone presents rather poor ORR activity with low $E_{1/2}$ values of 0.55 and 0.64 V, respectively. Despite the presence of Co SACs, CoP still displays limited ORR activity (0.69 V) due probably to severe molecular aggregation and low electrical conductivity. After non-covalently dispersing CoP molecules on conductive CNTs, a significant increase in $E_{1/2}$ is observed for CoP/CNT (0.80 V), affirming the positive role of the CNT support. This is also supported by loading C_{60} onto the CNTs to gain C_{60}/CNT, which gives a higher $E_{1/2}$ of 0.69 V than that of individual C_{60} and

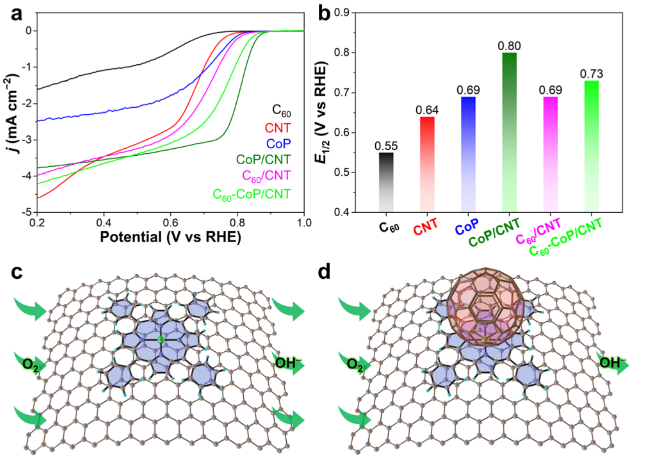

Fig. 2 (a) ORR polarization plots and (b) corresponding $E_{1/2}$ of the materials under study in 0.1 M KOH at 1600 rpm. Schematic illustrations of CoP/CNT (c) and C_{60}-CoP/CNT (d) that exhibit high and low ORR activities, respectively. Color code: C, cyan; N, blue; H, white; Co, green.

CNTs, in good line with the results of a previous study.[28] Rotating ring-disk electrode analysis reveals a highly-selective four-electron O_2-to-OH^- ORR pathway on CoP/CNT (Fig. S5, ESI†). More intriguingly, the further addition of C_{60} to CoP/CNT leads to an unexpected decrease of $E_{1/2}$ to 0.73 V, indicating an eminent ORR activity decay of Co SACs caused by C_{60} molecules. Due to the π–π stacking interactions, it is no wonder that CoP molecules are planarly adsorbed on the CNT surface, allowing O_2 reactants to be readily adsorbed to and reduced on the exposed Co sites, as illustrated in Fig. 2c. Once C_{60} molecules are introduced, they could be adsorbed to either CNTs or CoP owing to the analogous π–π stacking interactions. Given the deteriorated ORR activity of C_{60}-CoP/CNT and the aforesaid material characterization results, it is rationalized that C_{60} shall be situated on top of CoP, potentially blocking the access of O_2 to the ORR-active Co sites (Fig. 2d). On this account, C_{60} is not an expected facilitator, but rather can serve as a probe molecule to identify the active sites of SACs due to its site deactivation role.

Control experiments are carried out to verify the deactivation role of C_{60}. We first tune the molar ratio between CoP and C_{60} (0 : 1, 1 : 4, 1 : 2, and 1 : 1) of C_{60}-CoP/CNT. Polarization curves (Fig. 3a) and $E_{1/2}$ values (Fig. 3b) show that the ORR activity of C_{60}-CoP/CNT decreases from 0.80 to 0.73 V with the increase of the C_{60} content. Such positive correlation implies a growing inhibiting effect with more C_{60} molecules. Moreover, SCN^- is known as a probe that strongly binds to transition metals, causing chemical, physical, and electronic effects that dramatically disrupt the catalytic functions of such metals.[29–32] It is thus no surprise that the addition of SCN^- leads to a dramatic activity loss of CoP/CNT (Fig. 3c and d). However, the same $E_{1/2}$ reduction level by adding C_{60} as that by adding SCN^- strongly hints that C_{60} behaves just like SCN^- as an inhibitor to the Co SACs, indicating that C_{60} can serve as a similarly efficient probe to examine the catalytically active sites as SCN^-.

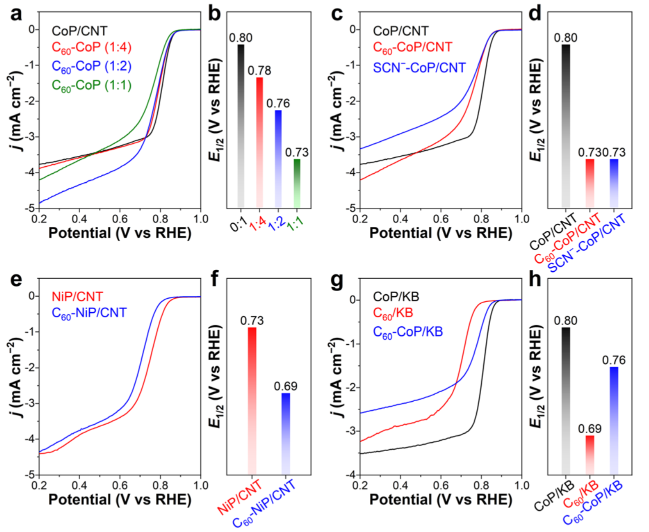

Fig. 3 (a) ORR polarization plots and (b) corresponding $E_{1/2}$ of CoP/CNT and C_{60}-CoP/CNT with different C_{60}/CoP ratios of 1 : 4, 1 : 2, and 1 : 1. (c) ORR polarization plots and (d) corresponding $E_{1/2}$ of CoP/CNT before and after the addition of C_{60} and SCN^-. (e) ORR polarization plots and (f) corresponding $E_{1/2}$ of NiP/CNT and C_{60}-NiP/CNT. (g) ORR polarization plots and (h) corresponding $E_{1/2}$ of CoP/KB, C_{60}/KB, and C_{60}-CoP/KB.

To rule out the potential influence of the exclusiveness of Co metal and the CNT support in the deactivation role of C_{60}, we have made further efforts by utilizing alternative MP molecules and a carbon support. Specifically, NiP/CNT and C_{60}-NiP/CNT are synthesized following the same synthetic recipe as that of the CoP counterparts. As displayed in Fig. 3e and f, substantial ORR activity loss is also observed for NiP/CNT after C_{60} adsorption with the $E_{1/2}$ values reduced from 0.73 to 0.69 V, again manifesting the role of C_{60} as an inhibitor. Analogously, a conductive carbon black, ketjenblack (KB), is adopted to replace CNTs as the support of CoP molecules following the same synthetic methods. It is discerned that CoP/KB and C_{60}/KB exhibit almost the same ORR activities as those of CoP/CNT and C_{60}/CNT (Fig. 3g and h). After the addition of C_{60}, CoP/KB also experiences dramatic ORR activity decay with an evidently decreased $E_{1/2}$ of 0.76 V. Therefore, it is confidently concluded that the probing role of fullerene will be universally applicable to various metal SACs and irrelevant to the carbon support.

Insights of the deactivation mechanism of C_{60} on CoP/CNT are further provided by DFT calculations. The preferable adsorption site of C_{60} on carbon-supported CoP is examined by calculating the binding energy (BE) of two distinct hybrids that have C_{60} and CoP on the same side (Fig. 4a) and opposite sides (Fig. 4b) of a graphene substrate, respectively. The results indicate that the hybrid with C_{60} adsorbed on top of CoP is more stable than the other by a ΔBE value of 0.435 eV. Even when the solvent effect is included in the computation, a more stable model is obtained for C_{60} adsorbed to CoP (a ΔBE value of 0.280 eV). Furthermore, O_2 adsorption to the Co site has to overcome the considerable interactions between C_{60} and CoP, as reflected by the elongated distance between Co and C_{60} after

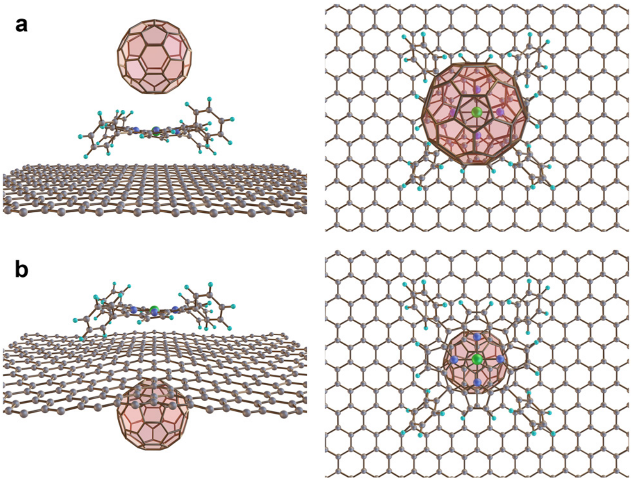

Fig. 4 Geometric configurations of C_{60} adsorbed on the same side (a) and opposite sides (b) of CoP adsorbed on a graphene matrix. Views of the atomic models from two distinct angles are illustrated on the left and right, respectively. Same color code as in Fig. 2.

O_2 binding (Fig. S6, ESI†). Combined with the above experimental results, it is interpreted that the molecular SACs have probably been spatially blocked by the C_{60} molecules that are favorably adsorbed on top of the ORR-active Co atoms, creating substantial steric hindrance to restrict the access of O_2. Note that the inhibiting role of C_{60} to SACs does not contradict with the previously reported positive effects brought to metal particle catalysts by C_{60} adsorption.[10–12] In fact, it rules out the possibility of the surface metal atom, to which the C_{60} molecule is specifically adsorbed, to serve as the potential active sites.

In summary, utilizing metalloporphyrin molecules that are uniformly dispersed on CNTs *via* non-covalent π–π interactions as model SACs, we disclose the probing role of C_{60} molecules in identifying the metal active sites of SACs towards the ORR. While the dispersion of CoP and C_{60} on CNTs leads to much superior ORR activities to bare CoP and C_{60}, respectively, the addition of C_{60} to CoP/CNT results in reduced ORR activity. A set of control experiments point out that the inhibiting effect of CoP gets severe with increasing C_{60} molar ratios. C_{60} leads to the same ORR activity decay as the recognized SCN^- poison. The probing role of C_{60} is also applicable to other metal SACs and carbon supports. Structural analysis and DFT calculations consistently indicate that the surface-stabilized CoP molecules are tightly confined between the C_{60} molecules and the basal plane of the CNTs. High steric hindrance is thus created to restrain the access of O_2 to the central metal atoms of MP SACs.

This work was supported by the National Natural Science Foundation of China (22301088, 21925104, 92261204) and the Hubei Provincial Natural Science Foundation of China (2022CFB623, 2021CFA020). The authors also acknowledge the support from the Analytical and Testing Center in Huazhong University of Science and Technology.

Data availability

The data supporting the findings of this study are available within the article and its ESI.†

Conflicts of interest

There are no conflicts to declare.

References

1 A. R. Puente Santiago, O. Fernandez-Delgado, A. Gomez, M. A. Ahsan and L. Echegoyen, *Angew. Chem., Int. Ed.*, 2021, **60**, 122–141.
2 K. Guo, N. Li, L. Bao and X. Lu, *Green Energy Environ.*, 2024, **9**, 7–27.
3 N. K. Gupta, A. Pashigreva, E. A. Pidko, E. J. Hensen and L. Mleczko, *et al.*, *Angew. Chem., Int. Ed.*, 2016, **55**, 1728–1732.
4 C. Zhang, W. Shen, K. Guo, M. Xiong and J. Zhang, *et al.*, *J. Am. Chem. Soc.*, 2023, **145**, 11589–11598.
5 N. Li, K. Guo, M. Li, X. Shao and Z. Du, *et al.*, *J. Am. Chem. Soc.*, 2023, **145**, 24580.
6 N. Li, M. Li, K. Guo, Z. Guo and R. Wang, *et al.*, *Adv. Energy Mater.*, 2024, **14**, 2401008.
7 M. F. Sanad, H. M. Franklin, B. A. Ali, A. R. Puente Santiago and A. N. Nair, *et al.*, *Angew. Chem., Int. Ed.*, 2022, **61**, e202116727.
8 T. Wang, L. Zhang, J. Wu, M. Chen and S. Yang, *et al.*, *Angew. Chem., Int. Ed.*, 2023, **62**, e202311352.
9 B. Peng, *J. Am. Chem. Soc.*, 2022, **144**, 19921–19931.
10 J. Zheng, L. Huang, C. H. Cui, Z. C. Chen and X. F. Liu, *et al.*, *Science*, 2022, **376**, 288–292.
11 B. Zhao, F. Chen, C. Cheng, L. Li and C. Liu, *et al.*, *Adv. Energy Mater.*, 2023, **13**, 2204346.
12 Y. Li, H. Zhang, T. Chen, Y. Sun and F. Rosei, *et al.*, *Adv. Funct. Mater.*, 2024, **34**, 2312970.
13 Y. Feng, X. Wang, J. Huang, P. Dong and J. Ji, *et al.*, *Chem. Eng. J.*, 2020, **390**, 124525.
14 Y. H. Choi, J. Lee, A. Parija, J. Cho and S. V. Verkhoturov, *et al.*, *ACS Catal.*, 2016, **6**, 6246–6254.
15 A. R. Puente Santiago, T. He, O. Eraso, M. A. Ahsan and A. N. Nair, *et al.*, *J. Am. Chem. Soc.*, 2020, **142**, 17923–17927.
16 A. Zitolo, V. Goellner, V. Armel, M. T. Sougrati and T. Mineva, *et al.*, *Nat. Mater.*, 2015, **14**, 937–942.
17 F. Luo, A. Roy, L. Silvioli, D. A. Cullen and A. Zitolo, *et al.*, *Nat. Mater.*, 2020, **19**, 1215–1223.
18 K. M. Zhao, S. Liu, Y. Y. Li, X. Wei and G. Ye, *et al.*, *Adv. Energy Mater.*, 2022, **12**, 2103588.
19 X. Yang, D. Xia, Y. Kang, H. Du and F. Kang, *et al.*, *Adv. Sci.*, 2020, **7**, 2000176.
20 P. Hutchison, P. S. Rice, R. E. Warburton, S. Raugei and S. Hammes-Schiffer, *J. Am. Chem. Soc.*, 2022, **144**, 16524–16534.
21 T. Zhang, J. Jin, J. Chen, Y. Fang and X. Han, *et al.*, *Nat. Commun.*, 2022, **13**, 6875.
22 M. L. Pegis, C. F. Wise, D. J. Martin and J. M. Mayer, *Chem. Rev.*, 2018, **118**, 2340–2391.
23 J. Wu and Y. X. Yu, *J. Colloid Interface Sci.*, 2022, **623**, 432–444.
24 J. Wu and Y. X. Yu, *Int. J. Hydrogen Energy*, 2023, **48**, 5961–5975.
25 C.-X. Zhao, B.-Q. Li, J.-N. Liu, J.-Q. Huang and Q. Zhang, *Chin. Chem. Lett.*, 2019, **30**, 911–914.
26 E. M. Perez and N. Martin, *Chem. Soc. Rev.*, 2015, **44**, 6425–6433.
27 A. J. Néel, M. J. Hilton, M. S. Sigman and F. D. Toste, *Nature*, 2017, **543**, 637–646.
28 R. Gao, Q. Dai, F. Du, D. Yan and L. Dai, *J. Am. Chem. Soc.*, 2019, **141**, 11658–11666.
29 S. Gupta, C. Fierro and E. Yeager, *J. Electroanal. Chem. Interfacial Electrochem.*, 1991, **306**, 239–250.
30 C. H. Bartholomew, *Appl. Catal., A*, 2001, **212**, 17–60.
31 M. S. Thorum, J. M. Hankett and A. A. Gewirth, *J. Phys. Chem. Lett.*, 2011, **2**, 295–298.
32 Q. Wang, Z. Y. Zhou, Y. J. Lai, Y. You and J. G. Liu, *et al.*, *J. Am. Chem. Soc.*, 2014, **136**, 10882–10885.